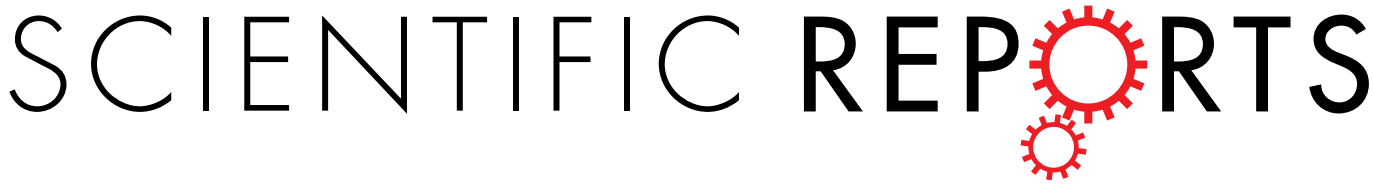

OPEN

Rotational friction of dipolar colloids measured by driven torsional oscillations

Received: 14 July 2016
Accepted: 05 September 2016
Published: 29 September 2016

Gabi Steinbach[1,2], Sibylle Gemming[1,2] & Artur Erbe[2]

Despite its prominent role in the dynamics of soft materials, rotational friction remains a quantity that is difficult to determine for many micron-sized objects. Here, we demonstrate how the Stokes coefficient of rotational friction can be obtained from the driven torsional oscillations of single particles in a highly viscous environment. The idea is that the oscillation amplitude of a dipolar particle under combined static and oscillating fields provides a measure for the Stokes friction. From numerical studies we derive a semi-empirical analytic expression for the amplitude of the oscillation, which cannot be calculated analytically from the equation of motion. We additionally demonstrate that this expression can be used to experimentally determine the rotational friction coefficient of single particles. Here, we record the amplitudes of a field-driven dipolar Janus microsphere with optical microscopy. The presented method distinguishes itself in its experimental and conceptual simplicity. The magnetic torque leaves the local environment unchanged, which contrasts with other approaches where, for example, additional mechanical (frictional) or thermal contributions have to be regarded.

Frictional forces play a fundamental role in the dynamics of mesoscopic objects, which are omnipresent in microfluidic and biological systems. The frictional interaction of moving objects with the viscous environment affects e.g. transport, demixing, diffusion, and propulsion[1–5]. The study of friction during these processes also gives access to the rheological and the aggregation behavior of colloids such as ferrofluids and gels[6–9]. In incompressible fluids, the key quantity is the Stokes friction coefficient f, which is the proportionality factor between the particle velocity and the drag force. Often, many-body effects in dense systems can be expressed as an expansion of the single-particle friction. An explicit, simple equation of f exists for single spheres in an ideally homogeneous medium by the Stokes law. Real systems, however, face deviations from that, caused either by a non-spherical object shape[10–15] or by anisotropic environments such as in non-ideal fluids or at surfaces/interfaces[16–20], e.g. in a cell or a microchannel[21–23]. As most of these problems cannot be solved analytically one relies on approximate solutions[24] or on experimental measurements. Friction from translational motion behaves differently from the friction during rotational motion[16,25,26]; for analysis sometimes both need to be decoupled[27,28]. Experimentally, the translational friction, f_t, can be simply derived from the spatial displacement of a diffusing particle via optical methods. Rotational friction, f_r, however, remains difficult to determine since additionally the orientation of the object has to be determined, which requires optical or shape anisotropy.

For nanoscopic objects, measurement methods rely on, e.g., scattering techniques[13,29,30], time-resolved phosphorescence spectroscopy[30], or internal reflection fluorescence microscopy[31]. In contrast, the study of microscopic objects is mainly limited to optical microscopy. One option is to measure the rotational diffusion with confocal microscopy[10,14,32] or holographic video microscopy[11,33], and then compute the friction via the Einstein–Smoluchowski relation. Another option is the application of a torque of known intensity by laser tweezers[16,34,35], or by mechanical micro-levers[36]. From the phase lag between rotor and drive one can derive f_r. While all these methods provide access to the rotational friction, a general drawback is that besides the technical expense they impose specific demands on the studied objects. For example, fluorescence labeling and a high resolution for diffusion measurements are required. When using optically or mechanically induced torques, the read-out of the phase difference between the drive and the rotator requires specific techniques, and moreover one has to correct for additional thermal or mechanical terms, which locally alter the friction coefficient.

[1]Institute of Physics, Technische Universität Chemnitz, 09107 Chemnitz, Germany. [2]Helmholtz-Zentrum Dresden-Rossendorf, Bautzner Landstrasse 400, 01328 Dresden, Germany. Correspondence and requests for materials should be addressed to G.S. (email: gabi.steinbach.de@gmail.com) or A.E. (email: a.erbe@hzdr.de)

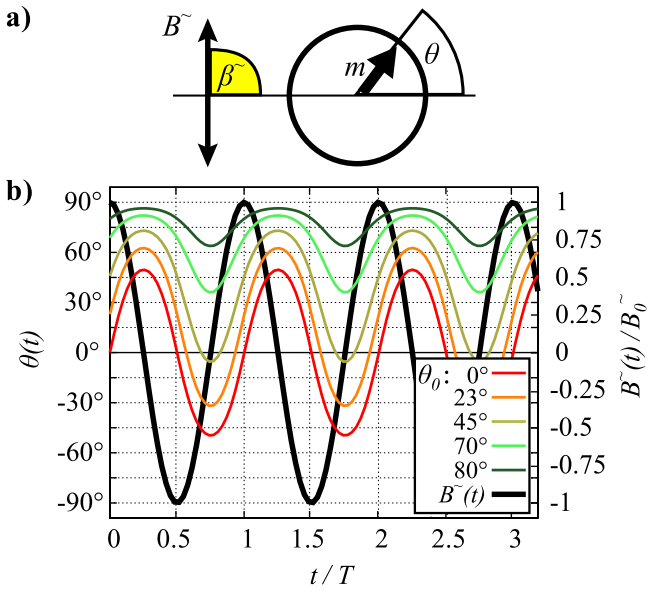

Figure 1. Oscillations in a uniaxial field. (**a**) Sketch of the dipolar particle with magnetic moment m in an oscillating field $B^{\sim}$. (**b**) Analytic functions of the angular oscillation $\theta(t)$ of a dipolar particle under a field $B^{\sim}$ according to equation (2) for different starting values θ_0, and the function of the applied field $B^{\sim}(t)$.

Here, we present a technically simple approach for measuring f_r of a single particle via light microscopy using oscillating magnetic torques. We drive dipolar particles with an oscillating field, which gives a time-dependent torsional oscillation angle $\theta(t)$ of the particles. The angular amplitude θ_A serves as the measurable quantity[37,38]. Experimentally, θ_A can be obtained, for example, with transmission light microscopy for particles with optical inhomogeneity[39–41]. As an advantage of this approach, the oscillation amplitude can be experimentally extracted easily from light microscopy even at low frame rates. Additionally, magnetic fields do not influence the local friction coefficient. The main difficulty of this approach is that the torsional motion can be expressed analytically only under uniaxial fields. In that case the particles, however, do not oscillate under well defined boundary conditions. We will, therefore, first explain this problem in uniaxial fields. Then, we demonstrate theoretically how the rotational Stokes friction coefficient of single dipolar microspheres can still be obtained from the amplitude of their torsional oscillation if they are driven by biaxial homogeneous fields. Based on numerical simulations, we discuss the relation between the oscillation amplitude and the friction coefficient, and derive an approximate solution $\theta_A(f_r)$ for the oscillation amplitude under biaxial fields. Finally, we demonstrate the applicability of this explicit equation in experimental studies. We determine the friction coefficient of single field-driven dipolar Janus microspheres from microscopy recordings.

Results

Uniaxial vs. biaxial field. In a highly viscous environment, where inertia can be neglected, the equation of rotation of a particle with magnetic moment $\mathbf{m}$ exposed to an external field $\mathbf{B}$ is obtained by balancing the magnetic torque, $\tau_m = \mathbf{m} \times \mathbf{B}$, against the viscous drag, $\tau_\nu = f_r \dot{\theta}$, with the angular velocity $\dot{\theta}$ of the particle.

We first consider a dipolar particle driven by a uniaxial, oscillating field $B^{\sim} = B_0^{\sim} \cos(\omega t)$ (Fig. 1a). We assume that the particle takes orientations θ in the value range $[-90°, \ldots, 90°]$ and that the field points along a radial field angle of $\beta^{\sim} = 90°$. In this case, the equation of rotational motion of is given by

$$f_r \dot{\theta}(t) = \mathbf{m} \times \mathbf{B}^{\sim} = mB_0^{\sim} \cos(\omega t) \sin(90° - \theta(t)) = mB_0^{\sim} \cos(\omega t) \cos\theta(t). \quad (1)$$

This differential equation has an analytic solution given by

$$\theta(t) = 2 \arctan \tanh \frac{2f_r \omega \operatorname{artanh}[\tan(\theta_0/2)] + mB_0^{\sim} \sin(\omega t)}{2f_r \omega}, \quad (2)$$

where θ_0 is the initial value of the radial orientation of the particle. θ_0 has no influence on the phase lag, which is exactly $\pi/2$, but θ_0 crucially impacts the form and the amplitude of the oscillation in a uniaxial, oscillating field (Fig. 1b). The dipolar particle performs a symmetric oscillation with respect to the ordinate only if the field is applied perpendicular to the initial orientation of the dipole. Here, this corresponds to $\beta^{\sim} = 90°$ and $\theta_0 = 0°$. The curve becomes asymmetric if $\theta_0 \neq 0°$. The form of the oscillation is, thus, strongly determined by θ_0. For a distribution of particles with random orientation θ_0 under a uniaxial, oscillating field, the amplitudes θ_A are, thus, not a distinct measure for the frictional drag. In a real system of colloidal particles additionally thermal fluctuations render an analysis difficult, because the fluctuations effectively alter θ_0 continuously. The fluctuation is most prominent when $B^{\sim}$ crosses zero during the oscillation, that is at low magnetic coupling parameters Γ, defined as the ratio between the magnetic interaction and the thermal energy.

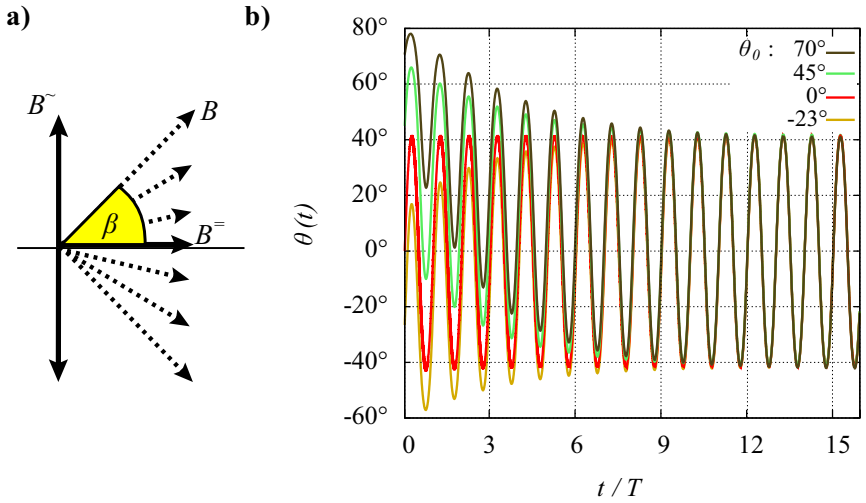

Figure 2. Oscillations in a biaxial field. (**a**) Sketch of the field vector B of a combined oscillating field $B^{\sim}$ and static field $B^{=}$. (**b**) Numerically calculated transient oscillation $\theta(t)$ of a dipolar particle in the biaxial field ($B^{\sim}$, $B^{=}$) for different starting values θ_0.

To quantitatively study the driven oscillation of single particles under well-defined boundary conditions, one has to ensure uniform oscillations and thermal fluctuations have to be suppressed by sufficiently large Γ values at all times. This can be realized if an oscillating magnetic field $B^{\sim} = B_0^{\sim} \cos(\omega t)$ is superimposed by a perpendicular static field $B^{=}$ (Fig. 2a). Note that here the orientation of the field changes periodically. The maximum field angle is $\beta = \arctan \frac{B_0^{\sim}}{B^{=}} < 90°$. On a dipolar particle, $B^{\sim}$ causes a radial oscillation $\theta(t)$ and $B^{=}$ exerts a permanent aligning torque that pulls the particle back to $\theta = 0°$. We assume the thermal energy to be sufficiently low if $\Gamma > 1000$, that is if $B^{=} \gtrsim \frac{1000 k_B T}{m}$. Under such a biaxial field, the torsional oscillation of a single particle is given by

$$f_r \dot{\theta}(t) = \mathbf{m} \times \mathbf{B}^{\sim} + \mathbf{m} \times \mathbf{B}^{=} \tag{3}$$

$$= mB_0^{\sim} \cos(\omega t) \cos\theta(t) + mB^{=} \sin\theta(t). \tag{4}$$

Unfortunately, there exists no analytic solution $\theta(t)$ for such a differential equation. From numerical calculations we have found that $B^{=}$ causes the dipole to always approach a symmetric steady-state oscillation through a transient oscillation (Fig. 2b). Then, the steady-state oscillation amplitude θ_A becomes independent of the actual initial orientation θ_0. For a particle with parameters m and f_r, the amplitude θ_A is uniquely defined for given values $B^{=}$, $B^{\sim}$, ω of the biaxial field. For that matter, θ_A in such a biaxial field can be used as a measure for the remaining system parameters m or f_r in equation (4). The only drawback in this approach is that there does not exist an analytic relationship between these system parameters and θ_A since equation (4) is not solvable. Instead, we derive an approximate function as presented below.

Oscillation amplitudes under biaxial fields. The oscillation amplitude θ_A depends on the interplay between the interaction of the dipole with the magnetic field and the frictional drag of the particle in the viscous medium. Assuming large values of $B_0^{\sim}/B^{=}$ such that $\beta = \arctan\left(\frac{B_0^{\sim}}{B^{=}}\right) \approx 90°$, the steady-state oscillation of a single particle can be approximated by the analytic solution, equation (2), of the oscillation in a uniaxial oscillating field ($B^{=} = 0$). In this case, the oscillation amplitude θ_A is given by

$$\theta_A^{\text{ana}} = 2 \arctan\tanh \frac{mB_0^{\sim}}{2f_r \omega}. \tag{5}$$

In the following, the impact of the field parameters $B^{=}$, $B_0^{\sim}$, ω on the oscillation amplitude θ_A of an ideal dipolar sphere and associated deviations from the analytic solution θ_A^{ana}, equation (5), for $\beta \neq 90°$ will be explained based on numerical simulations. For simplicity, we assume that $T = 0$ and do not incorporate thermal fluctuations in the simulations. The results are presented in Fig. 3a–c, where filled symbols correspond to numerically determined data points.

First, θ_A is presented as a function of the field amplitude $B_0^{\sim}$ (Fig. 3a). With increasing $B_0^{\sim}$ one can see that θ_A asymptotically approaches 90°. (The final convergence is not visible within the value range plotted in Fig. 3a, where the graphs reach only 85° at maximum.) The convergence is slowed down by increasing values of ω. In the case of vanishing frequency the curve reaches the limiting function $\theta_A \to \beta = \arctan \frac{B_0^{\sim}}{B^{=}}$, indicated as solid line in Fig. 3a. Next, the functional dependence of θ_A on ω is shown in Fig. 3b. Here, the field angle β is varied among

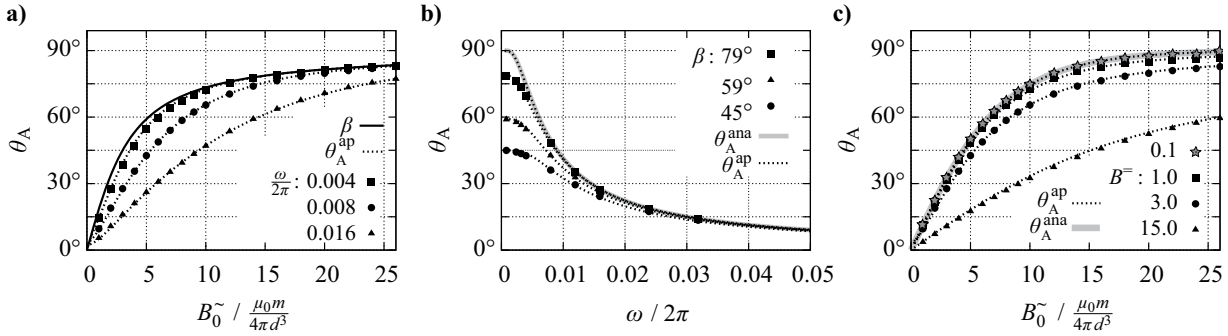

Figure 3. Numerical study of the oscillation amplitude θ_A as a function of the field parameters $B^{=}$, $B_0^{\sim}$, ω. Filled symbols correspond to numerically obtained points obtained for an ideal dipole with (**a**) $B^{=} = 3\frac{\mu_0 m}{4\pi d^3}$, (**b**) $B_0^{\sim} = 5\frac{\mu_0 m}{4\pi d^3}$, (**c**) $\omega/2\pi = 0.008$. Grey solid lines give the analytic curve θ_A^{ana} according to equation (5) and dotted lines correspond to approximate curves θ_A^{ap} according to equation (6) where $B^{=} \neq 0$.

the different data sets. In accordance with the trend in Fig. 3a, the amplitude θ_A decreases with increasing ω and converges to 0°. In the limit of $\omega = 0$, there is no oscillation and, thus, $\theta_A(\omega = 0) = \beta$ must hold. The variation of β results in a vertical compression or stretching of the curves $\theta_A(\omega)$. In the limit of $\beta = 90°$, which corresponds to vanishing $B^{=}$, the data points approach an upper limit given by the analytic solution θ_A^{ana}. Finally, the dependence $\theta_A(B_0^{\sim})$ is examined again, but now $B^{=} > 0$ is varied among the data sets while ω is kept constant (Fig. 3c). Again, θ_A increases with $B_0^{\sim}$ and asymptotically approaches 90°. The convergence becomes steeper if $B^{=}$ decreases. For the smallest value examined here $\left(B^{=} = 0.1\frac{\mu_0 m}{4\pi d^3}\right)$ the data points almost coincide with the analytic solution θ_A^{ana} in the absence of $B^{=}$, as indicated by the solid, grey curve. This proves that equation (5) provides a good approximation, assuming small values of $B^{=}/B^{\sim}$.

The analysis of the trends and of the boundary values of θ_A upon varying $B^{=}$, $B^{\sim}$ and ω provides suitable reference points for the search of a unique, approximate function $\theta_A^{ap}(B^{=}, B_0^{\sim}, \omega)$. Technically, the search must be based on the simulation data for which both system parameters, the magnetic moment m and the rotational friction coefficient f_r, are predefined input values. The detailed derivation of a suitable approximate function θ_A^{ap} is provided in the Supplementary Information in detail and will be summarized here only shortly. The key boundary conditions are that $\theta_A^{ap} = \beta = \arctan\frac{B_0^{\sim}}{B^{=}}$ must hold for vanishing ω and that equation (5) holds for vanishing $B^{=}$. An approximate expression can be obtained from a multiplication of both. Including some necessary correction factors we suggest that

$$\theta_A^{ap} = 2\ \arctan\ \tanh\frac{mB_0^{\sim}\cosh\sqrt{\frac{\pi}{2}\frac{B^{=}}{B_0^{\sim}}}}{2f_r\omega}\cdot\frac{2}{\pi}\arctan\frac{B_0^{\sim}}{B^{=}}. \quad (6)$$

Correction factors are indicated by red letters. The normalization factor $\frac{2}{\pi}$ accounts for the fact that the multiplication of equation (5) with $\arctan\frac{B_0^{\sim}}{B^{=}}$ leads to a value range of $\left[0: \left(\frac{\pi}{2}\right)^2\right]$ but it must hold that $\theta_A^{ap} \in \left[0: \frac{\pi}{2}\right]$. An additional adjustment term cosh[..] has been determined phenomenologically (Supplementary Information) to account for small deviations in the range of large β (Fig. S2, Table S1). Plotting θ_A^{ap} for the respective field parameters and the values $m = 1$ and $f_r = 100\frac{\mu_0 m^2}{4\pi d^3}$ used in the simulation (see Numerical Methods) shows a consistent agreement between the approximate function and the numerically obtained data sets (Fig. 3a–c). This indicates that equation (6) is a suitable approximation for the oscillation amplitude of a dipole in the applied biaxial field. This means in turn that from the measurement of θ_A under applied field values $B^{=}$, $B_0^{\sim}$, ω one can derive either dipole moment m or the Stokes friction coefficient f_r using equation (6).

Oscillation amplitudes of driven Janus colloids. Silica particles with a hemispherical magnetic coating, called Janus particles, enable the experimental study of rotational motion via transmission light microscopy[41,42]. The Janus director, which corresponds to the rotational symmetry axis of such particles, is visualized by the optical inhomogeneity between the coated and the uncoated hemispheres (Fig. 4). In the system studied here, the net magnetic moment of the particles points along the Janus director[39]. In this case the magnetic orientation of a particle coincides with the orientation of the optical contrast. We investigate particles with a diameter of $d = 4.54\,\mu$m after sedimentation in water on a substrate glass. The applied oscillating field $B^{\sim}$ points perpendicular to the substrate plane. Then the particles perform driven oscillations around an axis parallel to that plane. For such a radial oscillation, the orientation of a particle is obtained from the area ratio between the projection of the uncoated (bright) and the coated (black) hemisphere (Fig. 4). Note that due to the projection only the absolute value of θ_A can be extracted. The image analysis is limited to amplitudes $|\theta_A| \lessapprox 60°$ for the optical reasons of diffraction and total reflection.

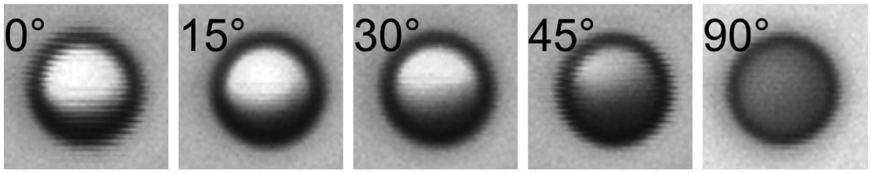

Figure 4. Microscopy images of a magnetic Janus particle with a diameter of 4.54 μm for different orientations θ. The ratio between the projected area of the transparent (bright) hemisphere and the coated (black) hemisphere serves as measure for the radial orientation θ of the particle.

The studied particles have a mean dipole moment of $m = 6.4 \cdot 10^9\,\mu_B$, which we have determined by SQUID magnetometry of an array of coated particles. In a constant field of $B^{=} \approx 0.01$ mT, they have a magnetostatic energy of $mB^{=} \approx 1440\,k_B T$, and, thus, thermal fluctuations are suppressed sufficiently at all times. Consequently, in combined fields $B^{=}$ and $B_0^{\sim}$, the non-interacting Janus particles oscillate uniformly after a transient time, and θ_A can be measured under well-defined conditions.

The data points obtained from measurements of Janus particles (Fig. 5) qualitatively show the same tendencies of θ_A as an ideal, dipolar sphere. Figure 5a shows that θ_A is an increasing function of $B_0^{\sim}$. An increase of ω results in a less steep increase of θ_A. This is proven explicitly by the trend that $\theta_A(\omega)$ decreases with increasing ω as shown in Fig. 5b for three different sets of field intensities. Experimental data sets with $\beta \approx 90°$ can be approximated by θ_A^{ana}, as well. Besides β and ω, also the maximum field intensity $B_0 = \sqrt{(B_0^{\sim})^2 + (B^{=})^2}$ affects θ_A. Exemplarily, we have measured θ_A for a set of field intensities B_0 with the same maximum field angle of $\beta = 35°$ (Fig. 5c). The experimental data points (unfilled symbols) show that θ_A converges to β with increasing B_0.

While the trends in the experimental (Fig. 5) and the numerical (Fig. 3) data compare well qualitatively, a quantitative comparison is not straightforward, because numerical time steps are not an equivalent of the real time. Consequently, the numerical and experimental values for the field frequency ω cannot be related to each other. At the end of this section we will show that a comparison is, however, possible if the experimental friction coefficient f_r is known, which will be determined next.

The coincidence in the trends of the experimental and the simulation data suggests that the model of a dipolar sphere reproduces the dynamics of single ferromagnetic particles. Therefore, equation (6) applies to the oscillation amplitude of the Janus particles also. Using this approximate function θ_A^{ap} we can extract the Stokes friction coefficient by fitting the experimental data sets in Fig. 5 via f_r. As noted already above, the friction of a particle rotating around an axis parallel to the substrate plane is examined here. The fit values f_r of the individual data sets with $B^{=} \gg 0$ are listed in Table 1 together with the applied field parameter values. The mean value amounts to $\overline{f_r} = 6.50 \cdot 10^{-19} \frac{\mathrm{kgm}^2}{\mathrm{s}}$ with a maximum deviation of 5% from that mean value. Using the fit values f_r and the given field values, the corresponding graphs θ_A^{ap} are plotted in Fig. 5. The curves show very good agreement with the trend of the experimental data. For comparison, for data sets with very small $B^{=}$ the curve θ_A^{ana} has been plotted in addition (Fig. 5b, grey solid lines). Apart from the range of very small ω, these curves coincide surprisingly well with those of θ_A^{ap}. This proves that for very small $B^{=}$ also the experimentally obtained amplitude θ_A is fairly well approximated by θ_A^{ana}.

The major source of error in this approach arises from the determination of the oscillation amplitude from the black-white ratio in the projected images of the particles. The measured ratio is very sensitive to the focus adjustment of the optical microscope. Deviations in the focus height from the one at which the calibration curve has been recorded directly cause an error of θ_A. From a number of reference measurements with seven particles each, we have determined an error of $\Delta\theta_A = \pm 4°$ that is achievable within the adjustment accuracy of our setup. The relative error of the friction value f_r for each data point (θ_A, $B^{=}$, $B^{\sim}$, ω) in Fig. 5 is then given by $\frac{\Delta f_r}{f_r} = \frac{1}{f_r}\frac{\partial f_r}{\partial \theta_A}\Delta\theta_A$, where the function f_r is obtained from solving equation (6) for f_r. This amounts to a maximum value of $\frac{\Delta f_r}{f_r} = 17\%$ for the data sets presented here.

Finally, the quantitative comparison between experiment and simulation can be conducted. The experimental field intensity, measured in mT, can be converted to the numerical unit $\frac{\mu_0 m}{4\pi d^3}$ of the field intensity by $1\,\mathrm{mT} \equiv 15.77\frac{\mu_0 m}{4\pi d^3}$ with the experimental values of m, d. As mentioned above, the full comparability requires a reference value for the numerical time steps. This can be obtained from the friction coefficient. While the real friction coefficient is measured in $\frac{kg\,m^2}{s}$, the numerical value has the dimension of energy, $\frac{\mu_0 m^2}{4\pi d^3} = 3.76 \cdot 10^{-18}\frac{kg\,m^2}{s^2}$. Thus, the ratio of both has the dimension of time in s. With the value used in the simulation, $f_r = 100\frac{\mu_0 m^2}{4\pi d^3} = 3.76 \cdot 10^{-16}\frac{kg\,m^2}{s^2}$, and the experimental mean value obtained from fitting, $\overline{f_r} = 6.50 \cdot 10^{-19}\frac{\mathrm{kgm}^2}{\mathrm{s}}$, this gives a numerical time step of $\Delta t = 1.73 \cdot 10^{-3}\,s$. An experimental frequency of $\omega/2\pi = 5$ Hz, thus, corresponds to a numerical frequency of $\omega/2\pi = 0.008$. Using this frequency and taking the field conversion into account, a quantitative comparison is possible. As an example, numerical data sets $\theta_A(B_0)$ of an ideal dipole for the case $\beta = 35°$ have been calculated and drawn in Fig. 5c (filled symbols). The agreement with the experimental data proves that the ideal dipolar particle is also a suitable model for the quantitative analysis of single dipolar Janus particles.

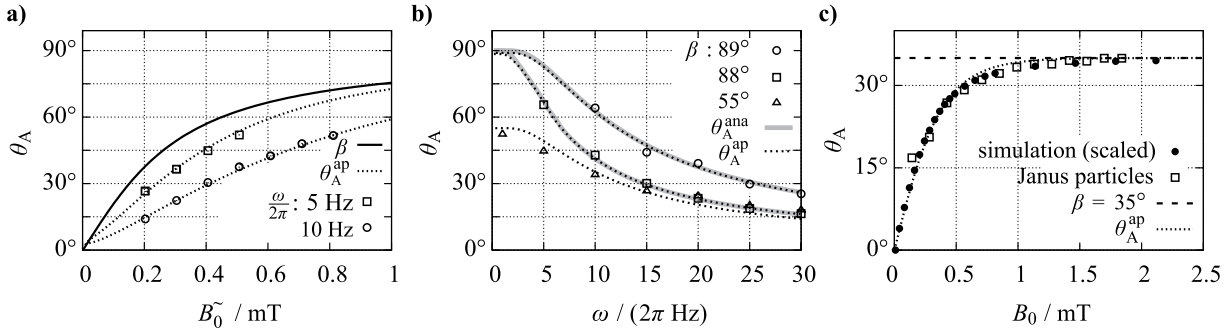

Figure 5. Experimental study of the oscillation amplitude θ_A as a function of the field parameters $B^{=}$, $B_0^{\sim}$, ω. Open symbols correspond to data points obtained experimentally for the Janus particles with (**a**) $B^{=} = 0.260\,\mathrm{mT}$, (**b**) for $\beta = 89°$ ($B_0^{\sim} = 1.015\,\mathrm{mT}$, $B^{=} = 0.017\,\mathrm{mT}$); 88° ($B_0^{\sim} = 0.607\,\mathrm{mT}$, $B^{=} = 0.017\,\mathrm{mT}$); 55° ($B_0^{\sim} = 0.558\,\mathrm{mT}$, $B^{=} = 0.390\,\mathrm{mT}$), (**c**) $\omega/2\pi = 5\,\mathrm{Hz}$. Grey solid lines give the analytic curve θ_A^{ana} given by equation (5) and dotted lines correspond to approximate curves θ_A^{ap} given by equation (6).

Figure 5 panel	Function	Field parameters			$f_r\left[10^{-19}\frac{\mathrm{kgm}^2}{\mathrm{s}}\right]$
(a)	$\theta_A(B_0^{\sim})$	$B^{=} = 0.260\,\mathrm{mT}$	$\omega/2\pi = 5\,\mathrm{Hz}$		6.49
		$B^{=} = 0.260\,\mathrm{mT}$	$\omega/2\pi = 10\,\mathrm{Hz}$		6.34
(b)	$\theta_A(\omega_B)$	$B^{=} = 0.390\,\mathrm{mT}$	$B^{\sim} = 0.558\,\mathrm{mT}$	($\beta = 55°$)	6.26
		$B^{=} = 0.017\,\mathrm{mT}$	$B^{\sim} = 1.015\,\mathrm{mT}$	($\beta = 89°$)	6.85
		$B^{=} = 0.017\,\mathrm{mT}$	$B^{\sim} = 0.607\,\mathrm{mT}$	($\beta = 88°$)	6.81
(c)	$\theta_A(B_0)$	$\beta = 35°$	$\omega/2\pi = 5\,\mathrm{Hz}$		6.27

Table 1. Values of the rotational friction coefficient f_r obtained from fitting the experimental data sets (Fig. 5a–c) of different dependencies (2nd column) to θ_A^{ap} or θ_A^{ana}, respectively, using the applied field parameters (3rd column).

Discussion

Here, we have presented a measurement tool for the rotational friction of single dipolar colloids. We have demonstrated that the friction coefficient can be obtained from the amplitude of driven torsional oscillations of the particles under biaxial magnetic fields. A semi-empirical equation has been derived that relates the oscillation amplitude with the friction coefficient. The validity of this equation has been tested experimentally with dipolar Janus spheres. For such particles with a diameter of $d = 4.54\,\mu\mathrm{m}$ in water on a glass substrate we have determined a value of $f_r = 6.50 \cdot 10^{-19}\frac{\mathrm{kgm}^2}{\mathrm{s}}$.

From such a measurement one can gain further insight into the studied system. Here, the distance between particle and substrate is accessible. According to the Stokes equation, $f_r = \pi\eta d^3$, ideally such a sphere in a homogeneous aqueous environment ($\eta = 1\,\mathrm{mPa\,s}$) has a rotational friction coefficient of $f_r^{\infty} = 2.94 \cdot 10^{-19}\frac{\mathrm{kgm}^2}{\mathrm{s}}$. The overestimation of the experimentally obtained value of f_r for the Janus particles is caused by their proximity to the substrate. The effect of the wall-particle distance on the rotational friction has been detailed in many previous studies[16,18–20,25,36]. According to the solution given by *Dean* and *O'Neill*[43], here, the wall-particle distance is approximately $0.01\,d$, which is $0.05\,\mu\mathrm{m}$. An additional, but small source for the difference between f_r and f_r^{∞} is given by the fact that the magnetic center is shifted radially away from the particle center[39] since the coating covers only one hemisphere. Since an externally applied torque acts on the magnetic center, the particle will rotate around a non-centric axis. This results in an increased effective hydrodynamic radius $r_H \sim f_r^{\infty}$ of the particles. In the presented experiment, this effect can, however not be separated from the influence of the surface. Based on the recorded videos we, however, suggest that this increase in r_H is very small since we could not measure it. Here, the influence of the non-spherical shape of the particle due to the coating can be neglected since the coating has a maximum height of less than 0.2%d.

A macroscopic equivalent of the discussed torsional oscillation of a sphere has been presented earlier[37] using cm-sized ferromagnetic spheres in a highly viscous fluid exposed to an oscillating magnetic field. There, the constant aligning torque has been realized by gravitational forces that act on a sphere with non-symmetric mass distribution. The authors reported similar qualitative behavior of the oscillation amplitude as we have discussed here. Therefore, we suggest that the concept of an approximate function for θ_A can be applied for a quantitative analysis in other systems. If gravitational forces are applied, then the magnetic moment and the torque-exerting field have to be replaced by the mass and the gravitational force accordingly.

In summary, the approximate equation θ_A^{ap} for the oscillation amplitude of a particle driven by superimposed oscillating and static fields provides an alternative, reliable method to measure the rotational Stokes friction coefficient f_r (or alternatively the net magnetic moment) of micron-sized Janus particles in a straightforward and

experimentally cheap way. The advantage of this method is that the application of a magnetic torque does not alter the frictional interaction between the object and the environment, and no corrections for additional energy contributions are necessary. Experimentally, the determination of the oscillation amplitude is the major source of measurement error, transferring into a relative error of $\frac{\Delta f_r}{f_r} \approx 17\%$ for the studied Janus particles. This error could, however, be considerably smaller for other particles for which the oscillation can be read out with higher precision.

The experimental study presented here discusses only spherical particles. This is, however, not a general limitation as the numerical study applies for any dipolar object, e.g., also ellipsoids[44–46] etc. Therefore, this method provides a promising tool in the growing subject of anisotropic magnetic particles in soft materials[47]. The effect of shape anisotropy of dipolar particles[48–51] on the rotational friction could be measured with the presented method. In addition, initially non-magnetic objects potentially can be studied after magnetic functionalization using recently promoted synthesis techniques based on microfluidics[52,53] or surface modification[40,54,55], which has been applied here[56]. In future, the presented method may provide a basis for the study of rotational friction in many-particle systems. From the difference between the oscillation amplitudes of single particles and of particles in dense suspension one could extract a quantitative analysis of the particle interaction. This concerns the change of the friction coefficient due to the modification of the hydrodynamic drag in the proximity to other particles, and the explicit interparticle interaction, e.g., the magnetic coupling. This promises an additional way to quantitatively analyze the numerously reported non-equilibrium systems of microscopic magnets such as chains, rods and filaments under time-dependent fields[39,45,46,57–60].

Methods

Numerical Methods. The rotational motion of a sphere with dipole moment m, that is exposed to a biaxial, orthogonal field, consisting of an oscillating field $B^{\sim} = B_0^{\sim} \sin(\omega t)$ and a static field $B^{=}$, has been calculated by numerically solving the equation of rotation (equation (4)). In this simulation, the particle is spatially fixed at its center. The orientation θ_{t+1} of the sphere at time step $t+1$ is obtained iteratively by

$$\theta_{t+1} = \theta_t + \frac{m}{f_r}(B_0^{\sim} \cos(\omega t) \cos\theta_t + B^{=} \sin\theta_t). \tag{7}$$

In the calculation, the magnetic moment is set to $m = 1$. A rotational friction coefficient of $f_r = 100\frac{\mu_0 m^2}{32\pi r_p^3}$ has been applied. It has the dimension of energy since the numerical time steps $\Delta t = (t+1) - t$ are dimensionless and set to 1. The angular frequency ω is also a dimensionless quantity.

Experimental Details. The particle preparation and experimental setup has been described in detail previously[39]. In short, silica spheres with a diameter of $d = (4.54 \pm 0.45)\,\mu$m have been coated on one hemisphere with a magnetic thin film according to an established recipe[56]. The coating consists a multilayer stack of Ta(3.0 nm)/Pd(3.0 nm) $[Co(0.28\,nm)/Pd(0.9\,nm)]_8$/Pd(1.1 nm). This stacking is known to exhibit strong magnetic anisotropy where the easy axis points perpendicular to the film surface[61]. When depositing such a film on a spherical particle, the anisotropy axis points perpendicular to the particle surface. After magnetic saturation, the film becomes single domain[62], which results in a radially symmetric anisotropy orientation across the particle surface[56]. This anisotropy distribution has been confirmed also theoretically[63]. Such a particle exhibits a stray field with dipolar characteristic, and the net dipole moment points perpendicular to the magnetic cap. A dilute suspension of such magnetically capped particles in distilled water is studied via transmission light microscopy. Following the density mismatch, the particles sediment on the bottom of the sample cell, which had been treated by plasma cleaning prior to sample preparation. To optimize the recording quality for digital image analysis, the microscopy illumination has been adjusted for homogeneous illumination via a condenser lense, and the sample has been aligned perpendicular to the light path using an adjustable stage. In addition, we have used a Lica objective (HC PL FL L 63x/0.70 CORR PH2) with an adjustable collar to correct for spherical aberration artifacts caused by the presence of the substrate glass. The attached digital camera (Leica DFC295) has a video resolution of 864 px × 648 px. An electromagnetic coil is mounted above the sample cell, providing perpendicular low-frequency fields. An additional set of two pairs of coils attached beneath the sample provide constant fields parallel to the sample plane. The microscopy recordings of single particles have been analyzed by optical image analysis using the open-source software ImageJ and the included plugin 'particle analysis'. After converting the recordings into black-white threshold bitmaps, the ImageJ plugin measures the projected area of the transparent hemisphere of a particle over several oscillation cycles. Due to the stroboscopic microscopy recording with low frame rate (20 fps), one obtains an overlaid beat of the oscillating curve area vs. time. The minimum value of the area is extracted and, using a calibration curve, this value is correlated with an oscillation amplitude θ_A.

References

1. Scholz, T. & Mandelkow, E. Transport and diffusion of tau protein in neurons. *Cell. Mol. Life Sci.* **71,** 3139–3150 (2014).
2. Mussel, M., Zeevy, K., Diamant, H. & Nevo, U. Drag of the cytosol as a transport mechanism in neurons. *Biophys. J.* **106,** 2710–2719 (2014).
3. Bleil, S., Marr, D. W. M. & Bechinger, C. Field-mediated self-assembly and actuation of highly parallel microfluidic devices. *Appl. Phys. Lett.* **88,** 263515 (2006).
4. Dreyfus, R. *et al.* Microscopic artificial swimmers. *Nature* **437,** 862–865 (2005).
5. Ebbens, S. J. & Howse, J. R. In pursuit of propulsion at the nanoscale. *Soft Matter* **6,** 726–738 (2010).
6. Abade, G., Cichocki, B., Ekiel-Jezewska, M. L., Nägele, G. & Wajnryb, E. Diffusion, sedimentation, and rheology of concentrated suspensions of core-shell particles. *J. Chem. Phys.* **136,** 104902 (2012).

7. Bossis, G., Kuzhir, P., López-López, M. T., Meunier, A. & Magnet, C. Importance of Interparticle Friction and Rotational Diffusion to Explain Recent Experimental Results. In *Rheology of Magnetic Suspensions* (ed. Wereley, N. M.) 1–30 (RSC Publishing, 2013).
8. Lee, J. T., Abid, A., Cheung, K. H., Sudheendra, L. & Kennedy, I. M. Superparamagnetic particle dynamics and mixing in a rotating capillary tube with a stationary magnetic field. *Microfluid. Nanofluidics* **13,** 461–468 (2012).
9. Dickinson, E. Structure and rheology of colloidal particle gels: Insight from computer simulation. *Adv. Colloid Interface* **199,** 114–127 (2013).
10. Edmond, K. V. *et al.* Tracking the brownian diffusion of a colloidal tetrahedral cluster. *Chaos* **21,** 041103 (2011).
11. Cheong, F. C. & Grier, D. G. Rotational and translational diffusion of copper oxide nanorods measured with holographic video microscopy. *Opt. Express* **18,** 6555–6562 (2010).
12. Han, Y. *et al.* Brownian motion of an ellipsoid. *Science* **314,** 626–630 (2006).
13. Hoffmann, M., Wagner, C. S., Harnau, L. & Wittemann, A. 3D Brownian diffusion of submicron-sized particle clusters. *ACS Nano* **3,** 3326–3334 (2009).
14. Hong, L., Anthony, S. M. & Granick, S. Rotation in suspension of a rod-shaped colloid. *Langmuir* **22,** 7128–7131 (2006).
15. Kraft, D. J. *et al.* Brownian motion and the hydrodynamic friction tensor for colloidal particles of complex shape. *Phys. Rev. E* **88,** 050301(R) (2013).
16. Leach, J. *et al.* Comparison of Faxen's correction for a microsphere translating or rotating near a surface. *Phys. Rev. E* **79,** 026301 (2009).
17. Donath, E. *et al.* Stokes friction coefficient of spherical particles in the presence of polymer depletion layers - analytical and numerical calculations, comparison with experimental data. *J. Chem. Soc. Faraday. Trans.* **93,** 115–119 (1997).
18. Liu, Q. L. & Prosperetti, A. Wall effects on a rotating sphere. *J. Fluid Mech.* **657,** 1–21 (2010).
19. Malysa, K. & Vandeven, T. G. M. Rotational and translational motion of a sphere parallel to a wall. *Int. J. Multiph. Flow* **12,** 459–468 (1986).
20. Goldman, A. J., Cox, R. G. & Brenner, H. Slow viscous motion of a sphere parallel to a plane wall. I: Motion through a quiescent fluid. *Chem. Eng. Sci.* **22,** 637–651 (1967).
21. Dettmer, S. L., Pagliara, S., Misiunas, K. & Keyser, U. F. Anisotropic diffusion of spherical particles in closely confining microchannels. *Phys. Rev. E* **89,** 062305 (2014).
22. Petrov, E. P., Petrosyan, R. & Schwille, P. Translational and rotational diffusion of micrometer-sized solid domains in lipid membranes. *Soft Matter* **8,** 7552–7555 (2012).
23. Levine, A. J., Liverpool, T. B. & MacKintosh, F. C. Dynamics of rigid and flexible extended bodies in viscous films and membranes. *Phys. Rev. Lett.* **93,** 038102 (2004).
24. Lee, S. H. & Leal, L. G. Motion of a sphere in the presence of a plane interface. II: An exact solution in bipolar coordinates. *J. Fluid Mech.* **98,** 193–224 (1980).
25. Cooley, M. D. A. On the slow rotation of a sphere about a diameter parallel to a nearby plane wall. *J. I. Math. Appl.* **4,** 163–173 (1968).
26. Cooley, M. D. A. & O'Neill, M. E. On slow motion generated in a viscous fluid by approach of a sphere to a plane wall or stationary sphere. *Mathematika* **16,** 37–49 (1969).
27. Edmond, K. V., Elsesser, M. T., Hunter, G. L., Pine, D. J. & Weeks, E. R. Decoupling of rotational and translational diffusion in supercooled colloidal fluids. *Proc. Natl. Acad. Sci. USA* **109,** 17891–17896 (2012).
28. Anthony, S. M., Kim, M. & Granick, S. Translation-rotation decoupling of colloidal clusters of various symmetries. *J. Chem. Phys.* **129,** 244701 (2008).
29. Rogers, S. A., Lisicki, M., Cichocki, B., Dhont, J. K. G. & Lang, P. R. Rotational diffusion of spherical colloids close to a wall. *Phys. Rev. Lett.* **109,** 098305 (2012).
30. Koenderink, G. H. *et al.* On the validity of Stokes-Einstein-Debye relations for rotational diffusion in colloidal suspensions. *Faraday Discuss* **123,** 335–354 (2003).
31. Kihm, K. D., Banerjee, A., Choi, C. K. & Takagi, T. Near-wall hindered brownian diffusion of nanoparticles examined by three-dimensional ratiometric total internal reflection fluorescence microscopy (3-D R-TIRFM). *Exp. Fluids* **37,** 811–824 (2004).
32. Sacanna, S., Rossi, L., Kuipers, B. W. M. & Philipse, A. P. Fluorescent monodisperse silica ellipsoids for optical rotational diffusion studies. *Langmuir* **22,** 1822–1827 (2006).
33. Wang, A. *et al.* Using the discrete dipole approximation and holographic microscopy to measure rotational dynamics of non-spherical colloidal particles. *J. Quant. Spectrosc. Radiat. Transfer* **146,** 499–509 (2014).
34. Bishop, A. I., Nieminen, T. A., Heckenberg, N. R. & Rubinsztein-Dunlop, H. Optical microrheology using rotating laser-trapped particles. *Phys. Rev. Lett.* **92,** 198104 (2004).
35. Lipfert, J., van Oene, M. M., Lee, M., Pedaci, F. & Dekker, N. H. Torque spectroscopy for the study of rotary motion in biological systems. *Chem. Rev.* **115,** 1449–1474 (2015).
36. Lobo, S., Escauriaza, C. & Celedon, A. Measurement of surface effects on the rotational diffusion of a colloidal particle. *Langmuir* **27,** 2142–2145 (2011).
37. Box, F., Thompson, A. B. & Mullin, T. Torsional oscillations of a sphere in a Stokes flow. *Exp. Fluids* **56,** 209 (2015).
38. Hollerbach, R., Wiener, R. J., Sullivan, I. S., Donnelly, R. J. & Barenghi, C. F. The flow around a torsionally oscillating sphere. *Phys. Fluids* **14,** 4192–4205 (2002).
39. Steinbach, G., Gemming, S. & Erbe, A. Non-equilibrium dynamics of magnetically anisotropic particles under oscillating fields. *Eur. Phys. J. E* **39,** 69 (2016).
40. Erb, R. M., Jenness, N. J., Clark, R. L. & Yellen, B. B. Towards holonomic control of Janus particles in optomagnetic traps. *Adv. Mater.* **21,** 4825–4829 (2009).
41. McNaughton, B. H. *et al.* Experimental system for one-dimensional rotational Brownian motion. *J. Phys. Chem. B* **115,** 5212–5218 (2011).
42. McNaughton, B. H. *et al.* Magnetic confinement of Brownian rotation to a single axis and application to Janus and cluster microparticles. *Appl. Phys. Lett.* **97,** 144103 (2010).
43. Dean, R. & O'Neill, M. E. A slow motion of viscous liquid caused by the rotation of a solid sphere. *Mathematika* **10,** 13–24 (1963).
44. Yan, J., Chaudhary, K., Bae, S. C., Lewis, J. A. & Granick, S. Colloidal ribbons and rings from janus magnetic rods. *Nat. Commun.* **4,** 1516 (2013).
45. Tierno, P., Claret, J., Sagues, F. & Cebers, A. Overdamped dynamics of paramagnetic ellipsoids in a precessing magnetic field. *Phys. Rev. E* **79,** 021501 (2009).
46. Guell, O., Sagues, F. & Tierno, P. Magnetically driven Janus micro-ellipsoids realized via asymmetric gathering of the magnetic charge. *Adv. Mater.* **23,** 3674–3679 (2011).
47. Tierno, P. Recent advances in anisotropic magnetic colloids: realization, assembly and applications. *Phys. Chem. Chem. Phys* **16,** 23515–23528 (2014).
48. Hurst, S. J., Payne, E. K., Qin, L. & Mirkin, C. A. Multisegmented one-dimensional nanorods prepared by hard-template synthetic methods. *Angew. Chem. Int. Ed.* **45,** 2672–2692 (2006).
49. Lee, S. H. & Liddell, C. M. Anisotropic Magnetic Colloids: A Strategy to Form Complex Structures Using Nonspherical Building Blocks. *Small* **5,** 1957–1962 (2009).
50. Ghosh, A. & Fischer, P. Controlled Propulsion of Artificial Magnetic Nanostructured Propellers. *Nano Lett.* **9,** 2243–2245 (2009).
51. Zhang, L. *et al.* Characterizing the Swimming Properties of Artificial Bacterial Flagella. *Nano Lett.* **9,** 3663–3667 (2009).

52. Chen, C. H., Abate, A. R., Lee, D. Y., Terentjev, E. M. & Weitz, D. A. Microfluidic assembly of magnetic hydrogel particles with uniformly anisotropic structure. *Adv. Mater.* **21,** 3201–3204 (2009).
53. Yuet, K. P., Hwang, D. K., Haghgooie, R. & Doyle, P. S. Multifunctional Superparamagnetic Janus Particles. *Langmuir* **26,** 4281–4287 (2009).
54. Smoukov, S. K., Gangwal, S., Marquez, M. & Velev, O. D. Reconfigurable responsive structures assembled from magnetic Janus particles. *Soft Matter* **5,** 1285–1292 (2009).
55. Sinn, I. *et al.* Magnetically uniform and tunable Janus particles. *Appl. Phys. Lett.* **98,** 024101 (2011).
56. Albrecht, M. *et al.* Magnetic multilayers on nanospheres. *Nat. Mater.* **4,** 203–206 (2005).
57. Yan, J., Bae, S. C. & Granick, S. Colloidal superstructures programmed into magnetic Janus particles. *Adv. Mater.* **27,** 874–879 (2015).
58. Martin, J. E. & Snezhko, A. Driving self-assembly and emergent dynamics in colloidal suspensions by time-dependent magnetic fields. *Rep. Prog. Phys.* **76,** 126601 (2013).
59. Swan, J. W., Bauer, J. L., Liu, Y. F. & Fürst, E. M. Directed colloidal self-assembly in toggled magnetic fields. *Soft Matter* **10,** 1102–1109 (2014).
60. Yan, J., Bloom, M., Bae, S. C., Luijten, E. & Granick, S. Linking synchronization to self-assembly using magnetic Janus colloids. *Nature* **491,** 578–581 (2012).
61. Carcia, P. F., Meinhaldt, A. D. & Suna, A. Perpendicular magnetic anisotropy in Pd/Co thin-film layered structures. *Appl. Phys. Lett.* **47,** 178–180 (1985).
62. Steinbach, G. *Ferromagnetic colloidal particles with anisotropic magnetization distribution: self-assembly and response to magnetic fields*. PhD thesis, Chemnitz University of Technology, 10–15, http://nbn-resolving.de/urn:nbn:de:bsz:ch1-qucosa-207403 (2016).
63. Ulbrich, T. C. *et al.* Magnetization reversal in a novel gradient nanomaterial. *Phys. Rev. Lett.* **96,** 077202 (2006).

Acknowledgements

The authors are grateful to Manfred Albrecht and Dennis Nissen for the preparation of the colloidal particles. This work was supported by the German Research Foundation (DFG) via Grant Nos ER 341/9-1, and FOR 1713 GE 1202/9-1.

Author Contributions

A.E. and G.S. conceived the experiments, G.S. and S.G. conceived the simulations, G.S. conducted the experiments and the simulations and analysed the results. All authors reviewed the manuscript.

Additional Information

Supplementary information accompanies this paper at http://www.nature.com/srep

Competing financial interests: The authors declare no competing financial interests.

How to cite this article: Steinbach, G. *et al.* Rotational friction of dipolar colloids measured by driven torsional oscillations. *Sci. Rep.* **6**, 34193; doi: 10.1038/srep34193 (2016).